A Godunov-type Finite-Volume Scheme for Flows on the Meso- and Micro-scales

Nash'at Ahmad*, Zafer Boybeyi† and Rainald Löhner‡
George Mason University, Fairfax, Virginia, 20030

and

Ananthakrishna Sarma§
Science Applications International Corporation, McLean, Virginia, 22102

A Godunov-type finite volume scheme based on unstructured adaptive grids is described for simulating flows on the meso-, micro- and urban-scales. The higher-order spatial accuracy is achieved *via* gradient reconstruction techniques after van Leer and the *total variation diminishing* condition is enforced with the help of slope-limiters. A multi-stage explicit Runge-Kutta time marching scheme is implemented for higher-order accuracy in time. The scheme is conservative and exhibits minimal numerical dispersion and diffusion. The sub-grid scale diffusion in the model is parameterized *via* the Smagorinsky-Lilly turbulence closure. Different benchmark and idealized test cases are simulated for the validation of the numerical scheme.

I. Introduction

The height of the Earth's atmosphere is orders of magnitude smaller compared to its circumference. Therefore the scale of horizontal flow is much larger than that in the vertical and the vertical pressure distribution is essentially hydrostatic. The small deviations from the hydrostatic balance due to temperature gradients across latitudes created by Earth's diurnal cycle, coupled with Coriolis force due its rotation act as the main drivers for atmospheric flows. On a broad scale, the atmospheric flows can be divided into hydrostatic and non-hydrostatic flows. Non-hydrostatic flows can span spatial scales ranging from several meters to several kilometers and time scales ranging from minutes to several hours. The hydrostatic flows in which the non-hydrostatic motions are embedded have scales that are orders of magnitude larger than the non-hydrostatic flows. This study focuses on the simulation of flows on the local scales, where the vertical spatial scales become comparable with the distances in the horizontal, and thus the hydrostatic flow model is no longer valid.

One interesting dilemma faced by the atmospheric modelers is the treatment of density. The density does not vary by much in the horizontal but in the vertical there are significant variations in density. Historically, the numerical modelers have preferred to treat the atmosphere as an incompressible fluid. This is true for nearly all of the current operational meso-scale models in use – e.g., the Regional Atmospheric Modeling System (RAMS)[32]. Although the incompressible/anelastic approximation has seen wide success, its limitations (the anelastic equation set is a subset of the fully-compressible equation set) have prompted atmospheric modelers to keep researching algorithms/methodologies for solving the fully compressible equation set[1, 24, 25]. It has been argued that the computational advantage of a larger time step in anelastic approximation is often overshadowed by the computational overhead involved in solving the elliptic equation for pressure at each time step. Furthermore, the anelastic approximation can fail to simulate processes in which the compressibility effects cannot be neglected, such as tornadoes[47] in which the Mach number can approach 0.5. The recent models for simulating non-hydrostatic flows have therefore used the compressible set of Navier-Stokes equations (e.g., Operational Multiscale Environment model with Grid Adaptivity (OMEGA) model[1] and the National Center for Atmospheric Research's (NCAR) current state-of-the-art Weather Research and Forecasting (WRF) model[36] use the fully compressible equation set).

---

* PhD Student, SCS, George Mason University, Fairfax, Virginia. AIAA Member.
† Associate Professor, SCS, George Mason University, Fairfax, Virginia.
‡ Professor, SCS, George Mason University, Fairfax, Virginia.
§ Senior Research Scientist, Science Applications International Corporation, McLean, Virginia.

Traditionally, finite difference discretizations of centered schemes such as the Leapfrog scheme have been favored for discretizing the atmospheric flow equation set. These types of schemes have large amounts of dispersion errors (non-physical spurious oscillations), which can contaminate the numerical results (see Figure 1). For synoptic scale models, it can be said that the computational efficiency of the Leapfrog scheme is more important than the calculation of accurate phase speed. The scheme is formally second-order accurate in both space and time and exhibits little numerical diffusion. At smaller spatial and temporal scales (non-hydrostatic meso-scale flows), large gradients of velocities and other physical quantities can develop and the local accuracy becomes important. The application of the Leapfrog scheme on smaller scales requires explicit time filtering for stability. The Asselin time filter, which is often used, degrades the accuracy of the scheme in time[13]. Furthermore, the scheme can introduce false negatives in important scalar microphysical quantities. To avoid false negatives either positive definite schemes[38] or Flux Corrected Transport (FCT)-type schemes[6] are sometimes used to advect scalar quantities.

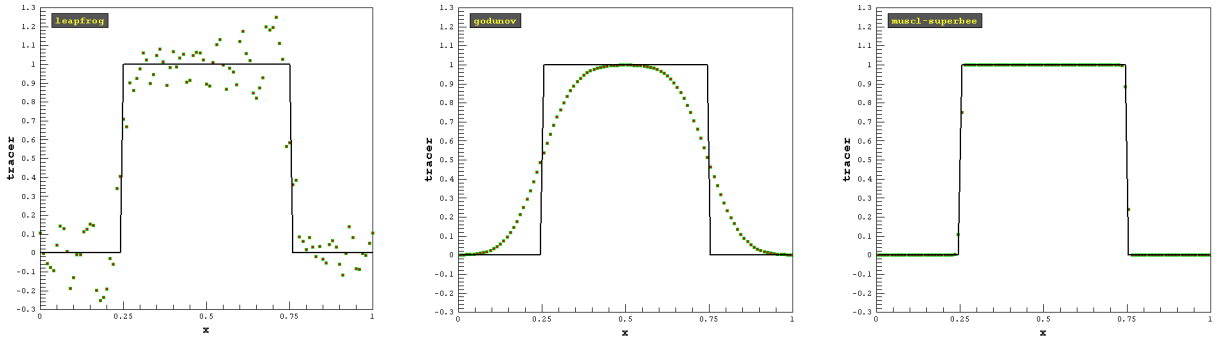

Leapfrog **Godunov** **MUSCL**

Figure 1. Comparison of different advection algorithms in 1D. Monotone Upstream centered Scheme for Conservation Laws[43] or MUSCL is the higher-order extension of the first-order Godunov scheme.

A number of studies have also been conducted in the past on the implementation of upwind schemes[38, 42]. The use of upwind schemes in operational models however has been limited. The upwind scheme is only first order accurate and therefore highly diffusive. Higher-order extensions of the upwind scheme can be computationally expensive[38] compared to, e.g., the Leapfrog scheme and that is why atmospheric modelers have paid little attention to its application for simulating atmospheric flows. In the past decades, there has been an immense increase in both CPU speed and available memory and these advances in computer hardware are projected to keep improving in the future. It is therefore not only feasible but also essential to explore the use of better numerical schemes including higher-order upwind schemes for atmospheric modeling. In this study high-resolution Godunov-type methods are explored for solving the non-linear equations arising in atmospheric flows. These finite volume discretizations are conservative and have the ability to resolve regions of steep gradients accurately, thus avoiding dispersion or phase errors in the solution.

Over the past two decades, Godunov-type methods[15] have gained wide popularity in the scientific computing community for solving the systems of hyperbolic conservation laws. Godunov's unique approach to numerical modeling of fluid flow is characterized by introducing physical reasoning in the development of the numerical scheme[44]. The construction of the scheme itself is based upon the physical phenomenon described by the equation sets. The scheme and its higher-order extensions have been used for high-speed flows/aerospace-related simulations[11, 28-29] and, for solving the shallow-water equations[45]. Ambitious attempts have been made to solve the complex set of hyperbolic equations arising in relativistic astrophysics[22]. Carpenter et al[10] have applied the method for atmospheric flows using an exact Riemann solver in conjunction with the Piecewise Parabolic Method[11]. Carpenter et al[10] show the inherent strengths of Godunov-type methods by providing a comparison with the Multidimensional Positive Definite Advection Transport Algorithm (MPDATA)[38] and the Leapfrog schemes. The important role Godunov-type methods can play in more accurately resolving atmospheric phenomena characterized by steep gradients is also pointed out.

Fronts, for example, are typically associated with large horizontal temperature and wind gradients and vertical wind shear. Strong convection in supercell thunderstorms can produce tornadoes, large hail, strong winds (in excess of 50 ms^{-1}), lightning and flash floods[9]. Drylines are characterized by a strong moisture gradient in the planetary boundary layer (e.g., in the Great Plains this gradient can be up to several degrees Celsius which is much larger than

the climatological average of 0.04 °Ckm^{-1} in the dewpoint temperature[35]). Drylines can trigger strong convective activity and winds in excess of 50 miles per hour have been observed. In tornadoes (F5 category), winds between 125 and 140 ms^{-1} have been observed. Hurricanes are yet another example of an atmospheric process which is characterized by extreme gradients of velocities and potential temperature[16].

In recent years, different authors have explored the possible use of the Godunov-type schemes for atmospheric modeling (*e.g.*, see Ref. 19, 21, 26 and 33). The application for atmospheric modeling however has been limited mostly to solving the atmospheric transport equation. In this study a high-resolution Godunov-type scheme for the Euler equations governing atmospheric flows is developed and then extended to the Navier-Stokes equations. This work differs from Carpenter et al's[10] work in the following aspects:

1) The conservative equation set for modeling compressible flows in the atmosphere is used, in which the conservation of energy is in terms of entropy-density instead of entropy.
2) The equations and the solution methodology are in the Eulerian frame of reference rather than Lagrangian.
3) An approximate Riemann solver is employed instead of an exact solver to calculate the Godunov fluxes. The computational cost of an exact Riemann solver can become prohibitive for simulations in three-dimensions. The solution obtained by an approximate Riemann solver is comparable to the solution from an exact solver – the computational overhead, however is greatly reduced.
4) The scheme is extended to the Navier-Stokes equations (the subgrid scale diffusion is treated as a source term) and implemented on unstructured meshes.

Traditionally atmospheric modelers have used structured grids with uniform spatial spacing in the horizontal. There are many advantages in using structured meshes – code-implementation and management is straightforward; discretization schemes can easily be extended to higher orders of accuracy; there is minimal computational overhead due to indirect accessing of data; and parallelization of the code is simple. The generation of structured meshes for complex geometries however is non-trivial and for practical applications (e.g., in CFD) most of the design-cycle time is spent on mesh-generation. The grid nesting technique is used to provide increased spatial resolution in the horizontal without requiring a fine mesh throughout the entire domain. This technique involves the sequential placement of multiple fine-scale meshes in the desired regions of the domain. Although the decision to spawn one or more sub-meshes is typically subjective and manually directed at the beginning of the simulation, many formulations have been developed to allow the sub-meshes to move with particular features in the flow, such as a hurricane. One major problem with this technique, however, is the interaction among multiple nested meshes, particularly the tendency for propagating waves to discontinuously change their speed upon passing from one nest to the next and to reflect off the boundaries of each nested mesh.

The unstructured grid technique has been widely used in other scientific disciplines[4, 27-28] for discretizing computational domains with complex geometries. It is a relatively new method for atmospheric science community that attempts to overcome the limitations of the structured grid technique. The primary benefit of the unstructured grid technique over a conventional structured grid lies in its ability to accurately discretize complex topologies with relative ease. Meshes for arbitrary surfaces and volumes in three dimensions can be generated. This capability is essential for resolving complex terrain features and shoreline boundaries for meso-scale and urban-scale atmospheric modeling. For flows on the urban and meso-scale, topographic forcing plays a dominant role in the development of the flow and an accurate representation of the underlying terrain is crucial for maintaining the fidelity of the numerical solution. A high degree of mesh refinement becomes critical in resolving locally driven flows, e.g., in simulating the flow field generated by an urban heat island[8].

In addition, computational efficiency can be achieved by providing variable and continuous resolution throughout the computational domain, with a high mesh resolution only in regions of interest. This feature of unstructured grid technique effectively removes the wave reflection problems that are common in grid-nesting techniques. Bacon et al[1] used unstructured meshes with static and dynamic adaptation for atmospheric modeling for the first time in the fully compressible and non-hydrostatic OMEGA model. The OMEGA model is based on unstructured prisms and has been applied to many atmospheric problems and validated extensively[7, 16]. A few other studies on the use of unstructured meshes for atmospheric applications have also been conducted in recent years (Ref. 5 and 14). With the exception of the OMEGA model, the atmospheric flow applications on unstructured grids have been limited to solving the scalar transport equation.

II. Governing Equations

The basic equations of fluid flow comprise of a set of partial differential equations for the conservation of mass (Continuity equation), the conservation of momentum, the conservation of energy and an equation of state to close

the system. The 2D Navier-Stokes equations governing atmospheric flows (see Ref. 1, 24, 25 and 31), written in the conservative form are as follows:

$$\frac{\partial U}{\partial t} + \frac{\partial F}{\partial x} + \frac{\partial G}{\partial y} = Q + D \tag{1}$$

Where,

$$U = \begin{bmatrix} \rho \\ \rho u \\ \rho v \\ \rho\theta \end{bmatrix}, \qquad F = \begin{bmatrix} \rho u \\ \rho u^2 + p \\ \rho uv \\ \rho u\theta \end{bmatrix}, \qquad G = \begin{bmatrix} \rho v \\ \rho uv \\ \rho v^2 + p \\ \rho v\theta \end{bmatrix} \tag{2}$$

ρ is the density of fluid, u is the velocity component in the x-direction, v is the velocity component in the y-direction and p is the pressure. If a parcel of air at temperature T and pressure p is subjected to an adiabatic compression or expansion to a final pressure of 10^5 Pa, then its potential temperature, θ is given by:

$$\theta = T\left(\frac{p_0}{p}\right)^{\frac{R_d}{C_p}} \tag{3}$$

Q is the source term and D is the diffusive flux term defined by:

$$D = K\nabla^2 U \tag{4}$$

In the momentum conservation equations, K is the sub-grid scale eddy diffusivity coefficient of momentum (= K_m). In the conservation of energy equation, the Laplacian of potential temperature is multiplied by the eddy diffusivity coefficient of heat (= K_h). For the sake of simplicity, the turbulent Prandtl number, Pr is set to unity:

$$\Pr = \frac{K_m}{K_h} = 1$$

The source term can be complex for atmospheric processes, and apart from body forces, may include terms for the heat sinks and sources produced due to the diurnal cycle of Earth, as well as microphysical processes of cloud formations and dissipations. For the purpose of this study, a simplified source term will be used. Atmosphere is assumed to be dry and the only source term is the gravitational force acting in the vertical direction. The system is closed by an equation of state for pressure,

$$p = C_0\ (\rho\theta)^{\gamma} \tag{5}$$

Where C_0 is a constant given by:

$$C_0 = \frac{R_d^{\gamma}}{p_0^{R_d/C_v}} \tag{6}$$

In the above relations, γ is the ratio of specific heats (= C_p/C_v = 1.4), R_d is the gas constant for dry air (= 287 J K^{-1} kg^{-1}), p_0 is the base state pressure (= 10^5 Pa). C_p (= 1004 J K^{-1} kg^{-1}) and C_v (= 717 J K^{-1} kg^{-1}) are the specific heats of air at constant pressure and volume respectively.

The Navier-Stokes equations contain both the advection and turbulent diffusion terms. The non-linearity due to the advective term and the parameterization of eddy diffusivity for the sub-grid scale diffusion, are the two main challenges in finding the numerical solution for these equations. In the current study, Smagorinsky's method[37] is

used for parameterizing the eddy viscosity. In the Smagorinsky turbulence closure, the sub-grid scale diffusion is parameterized in terms of the deformation tensor, D_{ij}:

$$D_{ij} = \frac{\partial u_i}{\partial x_j} + \frac{\partial u_j}{\partial x_i} - 2\frac{\delta_{ij}}{\delta_{ii}}\frac{\partial u_k}{\partial x_k} \tag{7}$$

For atmospheric flow simulations, Lilly[25], related the eddy viscosity coefficient, K_m to the total deformation in terms of the Richardson number, *Ri*:

$$K_m = \begin{cases} \frac{(c\Delta)^2}{\sqrt{2}}|Def|(1-Ri)^{0.5} & if \quad Ri < 0.25 \\ 0 & otherwise \end{cases} \tag{8}$$

Total deformation rate *Def* is defined as:

$$Def^2 = \frac{1}{2}\sum_i \sum_j D_{ij}^2 \tag{9}$$

The Richardson number *Ri* is defined as:

$$Ri = \frac{g}{\theta}\frac{\frac{\partial \theta}{\partial y}}{\left(\frac{\partial u}{\partial y}\right)^2} \tag{10}$$

The gravitational force, *g* is acting in the *y*-direction. The value of the Smagorinsky constant *c* is taken as 0.28. In two dimensions, Eq. (9) can be expanded as:

$$Def^2 = \left(\frac{\partial u}{\partial x} - \frac{\partial v}{\partial y}\right)^2 + \left(\frac{\partial u}{\partial y} + \frac{\partial v}{\partial x}\right)^2 \tag{11}$$

Where, $\left(\frac{\partial u}{\partial x} - \frac{\partial v}{\partial y}\right)$ is the *stretching deformation* and $\left(\frac{\partial u}{\partial y} + \frac{\partial v}{\partial x}\right)$ is the *shearing deformation*.

III. Numerical Scheme

In the absence of turbulent diffusion, the Coriolis effect, body forces and other sink/source terms, the Navier-Stokes equations reduce to the well-known set of Euler equations. The 1D Euler equations in the conservative form for an adiabatic atmosphere can be written as:

$$\frac{\partial U}{\partial t} + \frac{\partial F}{\partial x} = 0\,, \tag{12}$$

Where $\boldsymbol{U}$ is the vector of conserved variables:

$$U = \begin{bmatrix} u_1 \\ u_2 \\ u_3 \end{bmatrix} \equiv \begin{bmatrix} \rho \\ \rho u \\ \rho\theta \end{bmatrix}, \tag{13}$$

And $\boldsymbol{F}$ is the flux vector,

$$F = \begin{bmatrix} f_1 \\ f_2 \\ f_3 \end{bmatrix} \equiv \begin{bmatrix} \rho u \\ \rho u^2 + p \\ \rho u \theta \end{bmatrix} \tag{14}$$

The system is closed by an equation of state for pressure, Eqs. (5)-(6). The conservation laws in Eqs. (12)-(14) can be written in the discrete form as:

$$U_i^{n+1} = U_i^n + \frac{\Delta t}{\Delta x}\left[F_{i-\frac{1}{2}} + F_{i+\frac{1}{2}} \right] \tag{15}$$

bounded within a finite domain, $0 \le x \le L$, with appropriate initial and boundary conditions. Then, the Godunov flux is defined as,

$$F_{i+\frac{1}{2}} = F(U_{i+\frac{1}{2}}(0)) \tag{16}$$

where, $U_{i+\frac{1}{2}}(0)$ is the exact or approximate solution of the Riemann problem.

Godunov's method assumes piecewise constant data at cell centers. The Riemann problem is solved at each cell interface and the numerical flux is constructed from it. Thus, the global solution is a set of solutions of the local Riemann problems at each cell boundary (Figure 2), which is then evolved in time.

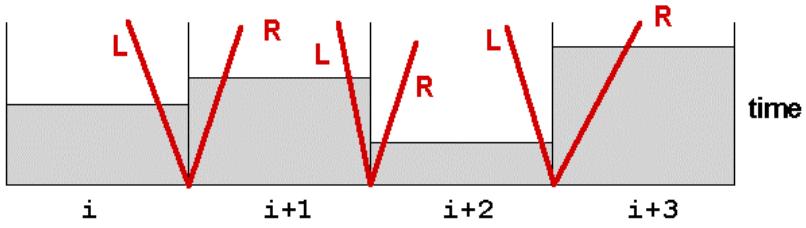

Figure 2. Piecewise constant data states within the computational cells. The discontinuities at cell boundaries form a set of local Riemann problems.

A. The Harten-Lax-van Leer-Contact Approximate Riemann Solver

The approximate Riemann solver Harten-Lax-van Leer-Contact (HLLC) is an extension of the HLL (Harten, Lax, and van Leer) solver by Toro[40-41]. In the original HLL Riemann approximation, the presence of contact discontinuities is neglected, which can give errors in the presence of shears within the flow. In Toro's extension (HLLC), the contact and shear waves are restored in the solution of the Riemann problem and it has the following three properties[29]:

1) Ability to resolve contact discontinuities and shear waves.
2) Positivity preservation of scalar quantities.
3) Enforcement of the entropy condition.

The solver has been successfully implemented with both explicit and implicit time-marching schemes and used for calculations of Euler as well as the Navier-Stokes equations[3]. The detailed derivation of the HLLC flux is given in Toro[40-41]. Here, the adaptation of the solver for Euler equations governing an adiabatic atmosphere is given. The flux at cell interface is defined as:

$$F^{HLLC} = \begin{cases} F_L, & if \quad S_L > 0 \\ F_L^*, & if \quad S_L \le 0 < S_* \\ F_R^*, & if \quad S_* \le 0 \le S_R \\ F_R, & if \quad S_R < 0 \end{cases} \tag{17}$$

where, S_L, S_*, *and* S_R are the signal velocities associated with the three waves in the solution of the Riemann problem. F_L and F_R flux vectors are given by:

$$F_L \equiv F(U_L) = \begin{pmatrix} (\rho u)_L \\ (\rho u^2)_L + p_L \\ (\rho\theta)_L \end{pmatrix}, \qquad F_R \equiv F(U_R) = \begin{pmatrix} (\rho u)_R \\ (\rho u^2)_R + p_R \\ (\rho\theta)_R \end{pmatrix} \tag{18}$$

The subscripts L and R denote the data states to the left and right of an interface (cell edge). The fluxes in the *starred* region are defined by:

$$F_L^* \equiv F(U_L^*) = \begin{pmatrix} S_* \rho_L^* \\ S_*(\rho u)_L^* + p_L^* \\ S_*(\rho\theta)_L^* \end{pmatrix} \tag{19}$$

and,

$$F_R^* \equiv F(U_R^*) = \begin{pmatrix} S_* \rho_R^* \\ S_*(\rho u)_R^* + p_R^* \\ S_*(\rho\theta)_R^* \end{pmatrix} \tag{20}$$

where,

$$U_L^* = \begin{pmatrix} \rho_L^* \\ (\rho u)_L^* \\ (\rho\theta)_L^* \end{pmatrix} = \frac{1}{S_L - S_*} \begin{pmatrix} (S_L - u_L)\rho_L \\ (S_L - u_L)(\rho u)_L + (p_L^* - p_L) \\ (S_L - u_L)(\rho\theta)_L \end{pmatrix} \tag{21}$$

and,

$$U_R^* = \begin{pmatrix} \rho_R^* \\ (\rho u)_R^* \\ (\rho\theta)_R^* \end{pmatrix} = \frac{1}{S_R - S_*} \begin{pmatrix} (S_R - u_R)\rho_R \\ (S_R - u_R)(\rho u)_R + (p_R^* - p_R) \\ (S_R - u_R)(\rho\theta)_R \end{pmatrix} \tag{22}$$

p^*_L and p^*_R are given by:

$$p_L^* = p_L + \rho_L (S_L - u_L)(S_* - u_L), \qquad p_R^* = p_R + \rho_R (S_R - u_R)(S_* - u_R) \tag{23}$$

B. Calculation of Signal Velocities

The minimum and maximum signal velocities present in the solution of the Riemann problem can be estimated directly from the wave speeds, S_L and S_R:

$$S_L = u_L - a_L \qquad S_R = u_R + a_R \tag{24}$$

The middle wave speed, S_*, was calculated using Batten's formulation[3], by setting $p^*_L = p^*_R$:

$$S_* = \frac{\rho_R u_R (S_R - u_R) - \rho_L u_L (S_L - u_L) + p_L - p_R}{\rho_R (S_R - u_R) - \rho_L (S_L - u_L)} \tag{25}$$

The subscripts L and R denote the data states on the left and right of a cell interface respectively.

C. Time-Marching

A four-stage explicit Runge-Kutta time integration scheme (Jameson et al[23]) is implemented to achieve higher-order accuracy in time. The scheme has relatively small memory requirements, is easy to implement and has been successfully used for obtaining both steady and unsteady solutions of the Euler as well as Navier-Stokes equations.

Let,

$$R_i \approx \frac{\partial U}{\partial t} \tag{26}$$

Then the four-stage Runge-Kutta time-marching scheme can be written as:

$$\begin{aligned} U_i^{(0)} &= U_i^n \\ U_i^{(1)} &= U_i^{(0)} - \alpha_1 \Delta t R_i^{(0)} \\ U_i^{(2)} &= U_i^{(0)} - \alpha_2 \Delta t R_i^{(1)} \\ U_i^{(3)} &= U_i^{(0)} - \alpha_3 \Delta t R_i^{(2)} \\ U_i^{(4)} &= U_i^{(0)} - \alpha_4 \Delta t R_i^{(3)} \\ U_i^{n+1} &= U_i^{(4)} \end{aligned} \tag{27}$$

Where, $\alpha_1 = 1/4$, $\alpha_2 = 1/3$, $\alpha_3 = 1/2$ and $\alpha_4 = 1$, are the Runge-Kutta constants. During the time integration, the local Riemann solution on one interface should not be allowed to interfere with the Riemann solution on another interface. If the interference of waves occurs then, the solution of the Riemann problem can no longer be considered local. This forms the basis of the Courant restriction on the Godunov method. The time step is calculated by finding the maximum wave speed in each cell:

$$\Delta t = CFL \cdot \frac{\Delta x}{abs(u) + a} \tag{28}$$

D. Solver Algorithm

The solution algorithm for constructing Godunov-type schemes *via* the HLLC Riemann solver can be summarized as follows:

1) Given the left and the right data states across each cell interface, calculate the signal velocities, S_L, S_*, and S_R by Eqs. (24)-(25).
2) Construct the Godunov flux obtained from the HLLC approximate Riemann solver using Eqs. (17)-(23).
3) Evolve the set of conservative variables in time using Eqs. (26)-(27) with the time step restricted by Eq. (28).

E. Implementation on Unstructured Meshes

The solver is implemented on unstructured meshes in two-dimensions. The convective/advective fluxes are calculated by summing all the incoming and outgoing fluxes through each face of the control volume. Eq. (1)-(2) can be written in the integral form as:

$$\frac{d}{dt}\int_{\Omega} U \, d\Omega = -\oint_{\Gamma} (F, G).n \, d\Gamma \tag{29}$$

Where, **n** is the unit normal pointing out of the control surface Γ of the control volume Ω. Figure 3 shows the cell-centered control volume, Ω with each of its control surfaces and the unit normals pointing outwards from the control surfaces. Eq. (29) can be approximated directly:

$$V_{cell} \frac{du_{cell}}{dt} + \sum_{faces} (F, G) \cdot s = 0 \tag{30}$$

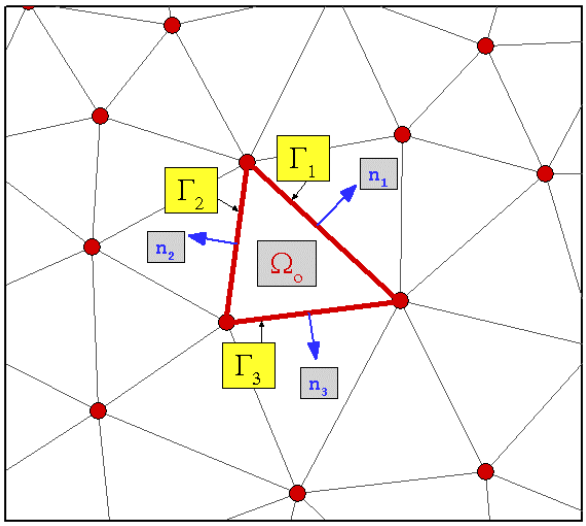

Figure 3. Cell-centered control volume Ω_o and its control surfaces, Γ_i. The unit normals n_i, should always point outwards from the control volume.

Where V_{cell} is the volume of the control volume (area of the triangle in the case of the two-dimensional triangular mesh), u_{cell} is the cell-averaged value of u at cell center and s is the control surface area (edge lengths of the triangle in case of the two-dimensional mesh). The calculation of fluxes using Godunov's method in conjunction with the HLLC Riemann solver was described in detail in previous sections. For the unstructured mesh, the implementation of the method is straightforward. The flux across each edge of the cell is calculated using Godunov's method. The values on either side of a cell edge form the initial conditions for the Riemann problem. The solution is marched in time within the multi-stage Runge-Kutta time marching scheme. In a loop over edges the values of cells on either side of the edge are used to calculate the fluxes. Once the fluxes have been calculated, they are added to the cell centered value in a loop over cells. For the second-order calculation gradient-limited extrapolated values are used in the Riemann solver instead of cell averages. Both the Green-Gauss and the Linear Least-Squares gradient reconstruction[2] techniques have been implemented to extend the spatial accuracy of scheme to higher-order. The scheme is made TVD[17] with the help of slope limiters[2]. The Laplacian operator is calculated using the method suggested by Holmes and Connell[18].

IV. Results

A. Doswell's Frontogenesis

The simulation of Doswell's frontogenesis problem (Doswell[12]; Suratanakavikul and Marquis[39]) is presented in this section. Doswell's idealized model describes the interaction of a non-divergent vortex with an initially straight frontal zone. An exact solution is readily available for this case, which makes it ideal for a quantitative as well as qualitative validation of a numerical scheme. The flow field was defined as follows:

$$u(x,y) = -\frac{y}{r}\frac{f_t}{f_{\max}}; \quad v(x,y) = \frac{x}{r}\frac{f_t}{f_{\max}} \tag{31}$$

where, r is the distance from any given point to the origin of the coordinate system, $f_{max} = 0.385$ is the maximum tangential velocity and f_t is given by:

$$f_t = \frac{\tanh(r)}{\cosh^2(r)} \tag{32}$$

The domain was bounded within x:[-4,4] and y:[-4,4]. The simulation was run for $t = 4$ units. The evolution of tracer field in time t, is given by the exact solution:

$$q(x,y,t) = -\tanh\left[\frac{y}{2}\cos(f\cdot t) - \frac{x}{2}\sin(f\cdot t)\right] \tag{33}$$

where, $f = \frac{1}{r}\frac{f_t}{f_{\max}}$. The initial tracer field can be obtained from Eq. (33) by setting $t = 0$:

$$q(x,y,0) = -\tanh\left(\frac{y}{2}\right) \tag{34}$$

Figure 4 shows the initial conditions for the Doswell Test and a comparison between the exact and the numerical solution is given in Figure 5. In addition several simulations were conducted to compare solutions on different types of meshes using different gradient-reconstruction techniques. The error in solution was defined as:

$$rms\ \ error = \frac{\sqrt{\sum_{1}^{nelem}\left|q_{simulated}(x,y) - q_{exact}(x,y)\right|^2}}{nelem} \tag{35}$$

Figure 6 shows the computed results for time = 4 units on different meshes. Only a zoomed view of the mesh center is shown in the figure. Mesh 1 consists of right angle triangles; Mesh 2 is a standard unstructured mesh in which an effort has been made to ensure good quality of triangles. Mesh 3 is similar to Mesh 2 except that smoothing is not performed. Mesh 3 is the worst of the three in terms of quality. The error in solution compared to the exact solution is plotted in Figure 7. The first-order solution on Mesh 2 is also shown for comparison. Although the error in the higher-order solution is low for all three meshes, the differences in accuracy due to mesh quality and the type of reconstruction technique used are clearly demonstrated. Mesh 2 (best quality mesh) performs much better than the other two meshes and the Linear Least-Squares technique gives more accurate results than the Green-Gauss reconstruction technique. It is interesting to note that the Green-Gauss for Mesh 1 gives the worst results. This is due to the fact that Green-Gauss technique is second-order accurate only for equilateral triangles and Mesh 1 comprises of only right angle triangles.

A convergence study was performed to formally determine the accuracy of the high-resolution MUSCL scheme. The scheme was also compared with the Leapfrog and the Lax-Wendroff schemes. For consistency, the time marching in the MUSCL comprised of the 2-stage Runge-Kutta scheme. The comparison is shown in Figure 8 (left panel). The MUSCL scheme has lower RMS error than both the Leapfrog and the Lax-Wendroff schemes at different mesh resolutions. The L_2 error is plotted in Figure 8 (right panel). A maximum slope of 1.67 (Figure 8-right panel) on the log-log plot indicates that the higher-order scheme is not formally second-order accurate. This impression can be misleading. In the presence of discontinuities TVD schemes revert to first-order locally, which can degrade the overall order of accuracy for the scheme and not necessarily the accuracy of the scheme itself. It has been shown that even in the absence of discontinuities, for calculating smooth solutions, the TVD schemes do not formally show a convergence rate of 2. This is due to the fact that limiters clip local extremas to preserve monotonicity. Venkatakrishnan[46] reports an order of accuracy of 1.65 for various monotonic schemes (for solving the linear scalar advection equation) which are formally second-order accurate.

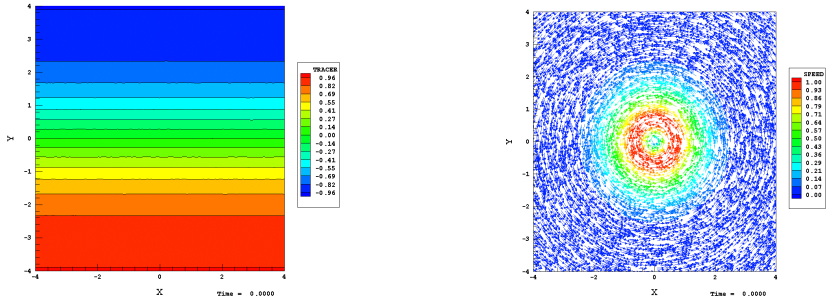

Figure 4. Doswell's Frontogenesis. Initial frontal zone (left) and the vortex defining the flow field (right).

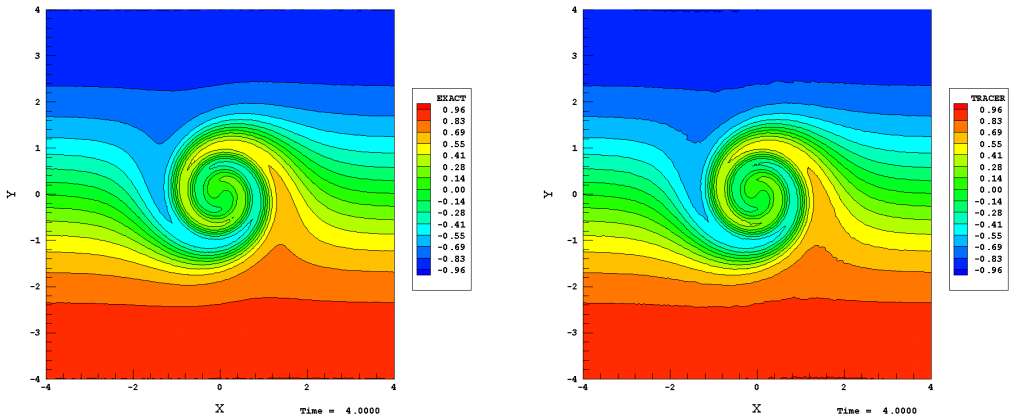

Figure 5. Doswell's Frontogenesis. Exact solution of the tracer field at time = 4 units (left) and the corresponding simulation result *via* MUSCL (right).

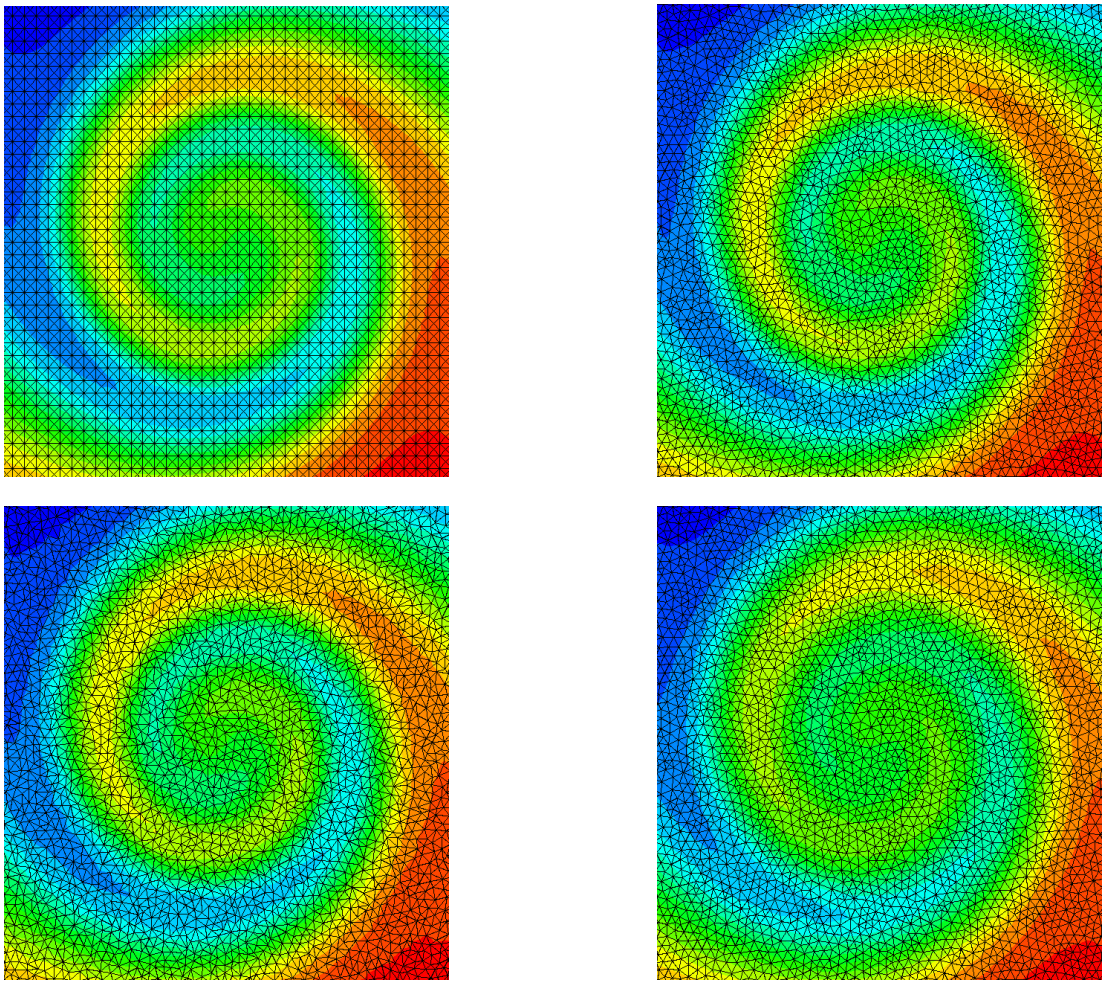

Figure 6. Higher-order solution on Mesh 1 (top left), Mesh 2 (top right), Mesh 3 (bottom left) and first-order solution on Mesh 2 (bottom right).

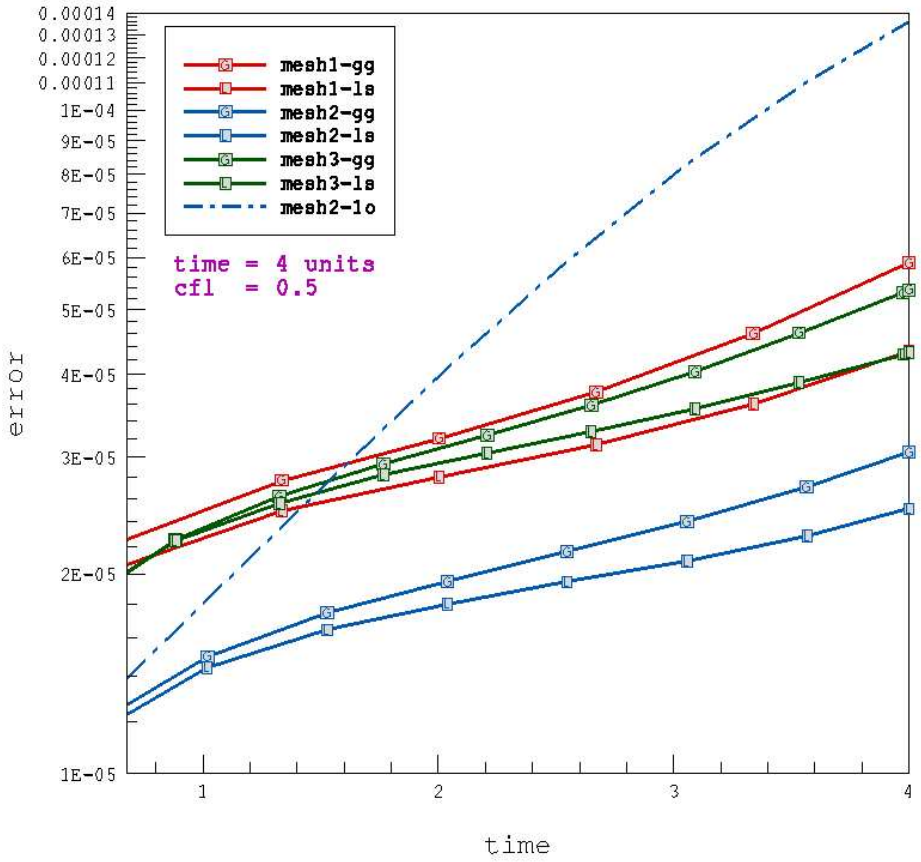

Figure 7. Doswell's Frontogenesis. Error in solution for different meshes, reconstruction methods and order of numerical scheme.

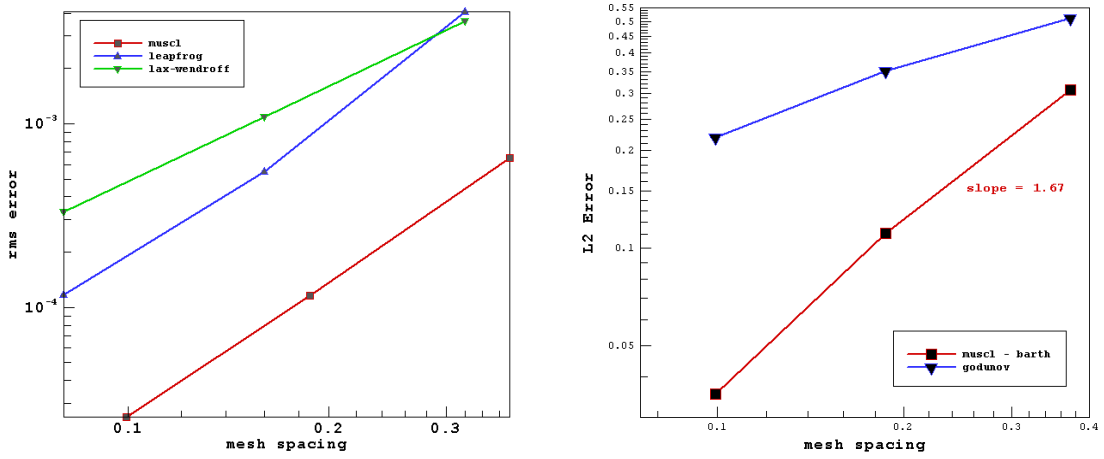

Figure 8. Comparison of the MUSCL scheme on unstructured triangular mesh with the Leapfrog and Lax-Wendroff schemes on structured rectilinear grid (left). Figure on the right shows that the higher-order scheme converges at a rate of 1.67 which is almost twice the rate of the first-order Godunov scheme.

B. Convection in Neutral Atmosphere

Simulation of a buoyant thermal is described in this section. The set of Navier-Stokes equations in two dimensions was solved for this problem. Model was initialized by introducing a warm bubble with a diameter of 500 m and a constant potential temperature of 0.5 degrees higher than the surrounding environment (neutral atmosphere in hydrostatic balance with a uniform potential temperature of 300 K). A 1km x 1km domain was defined for the simulation. The pressure was re-adjusted for hydrostatic equilibrium after the introduction of the thermal. The variables were first initialized on a structured grid and then interpolated to the unstructured mesh using bilinear interpolation. It should be noted that initializing a perfect hydrostatic balance on an unstructured mesh is non-trivial and the interpolation from the structured grid to the unstructured grid introduces errors (i.e., hydrostatic imbalances in the initial state of the atmosphere) in the initial conditions. All domain boundaries were treated as solid walls. The unstructured triangular mesh consisted of 39386 triangular elements with edge lengths varying from 3.5 m to 12.4 m.

Shear is generated due to gradients in the flow normal to its direction and often results in instabilities. In stratified fluids (e.g., the atmosphere) the instabilities due to shear are damped out by the stratification. The Miles theorem predicts the transition from stable to unstable flow and the onset of the Kelvin-Helmholtz instability for low Richardson numbers ($Ri < 0.25$). Usually a high Richardson number implies stability and instabilities in flow are expected at low Richardson numbers. The Kelvin-Helmholtz type of instability is common in the atmosphere and has been observed in billow clouds. The breaking of waves in the Kelvin-Helmholtz instability can generate the clear air turbulence (CAT) in the atmosphere.

The objective of this model validation run was to simulate the onset of the Kelvin-Helmholtz type of instability in the atmosphere. In the absence of an analytical solution, the test can evaluate the scheme only in qualitative terms. This evaluation however, provides valuable information on the scheme's ability to simulate the fundamentals of atmospheric thermodynamics and dynamics. Buoyant thermals are highly nonlinear phenomena and therefore, the detailed structure of the evolving thermal is dependent on the type of model formulation itself[10] (i.e., the equation set used – compressible, quasi-compressible, anelastic, etc.). Nonetheless, there are certain features, which are expected in the resulting flow field. The introduction of the thermal in the domain generates acceleration in the center of the bubble accompanied by downdrafts on the either side of the bubble. As the buoyant thermal rises, a shear layer is developed at the lateral edges of the thermal. Initially the atmosphere is strongly stratified which damps out the onset of flow instabilities, but as the thermal rises, the weakening of stratification at the edge of the thermal triggers the onset of the instability. Figures 9-11 show the time evolution of potential temperature gradient, shear, the Richardson number (scaled from –0.26 to 0.26; the values greater than 0.26 are set to zero) and potential temperature. The generation of shear layer and weakening of stratification resulting in the Kelvin-Helmholtz type of instability can be seen in the figures. The vectors in the figures represent only the flow direction.

V. Conclusion

This work has opened up the door for future use of high-resolution Godunov-type methods for atmospheric flow simulations on unstructured meshes. The scheme shows promise in simulating flows characterized by steep gradients on the meso- micro- and urban-scales. The use of unstructured grids provides the ability to simulate the complex, multi-scale atmospheric flows in a computationally efficient manner and solution-adaptive techniques can easily be implemented. However, there is much room for improvement. For example, better CPU performance provided by implementing an implicit time-marching scheme (Luo, et al[30]; Sharov, et al[34]) can further increase the robustness of the flow solver. Inclusion of more physics (microphysics, radiation schemes and surface layer physics) is needed for simulating realistic flows. The role of various limiters (Venkatakrishnan[46]) and especially multidimensional limiters (Hubbard[20]) needs to be explored.

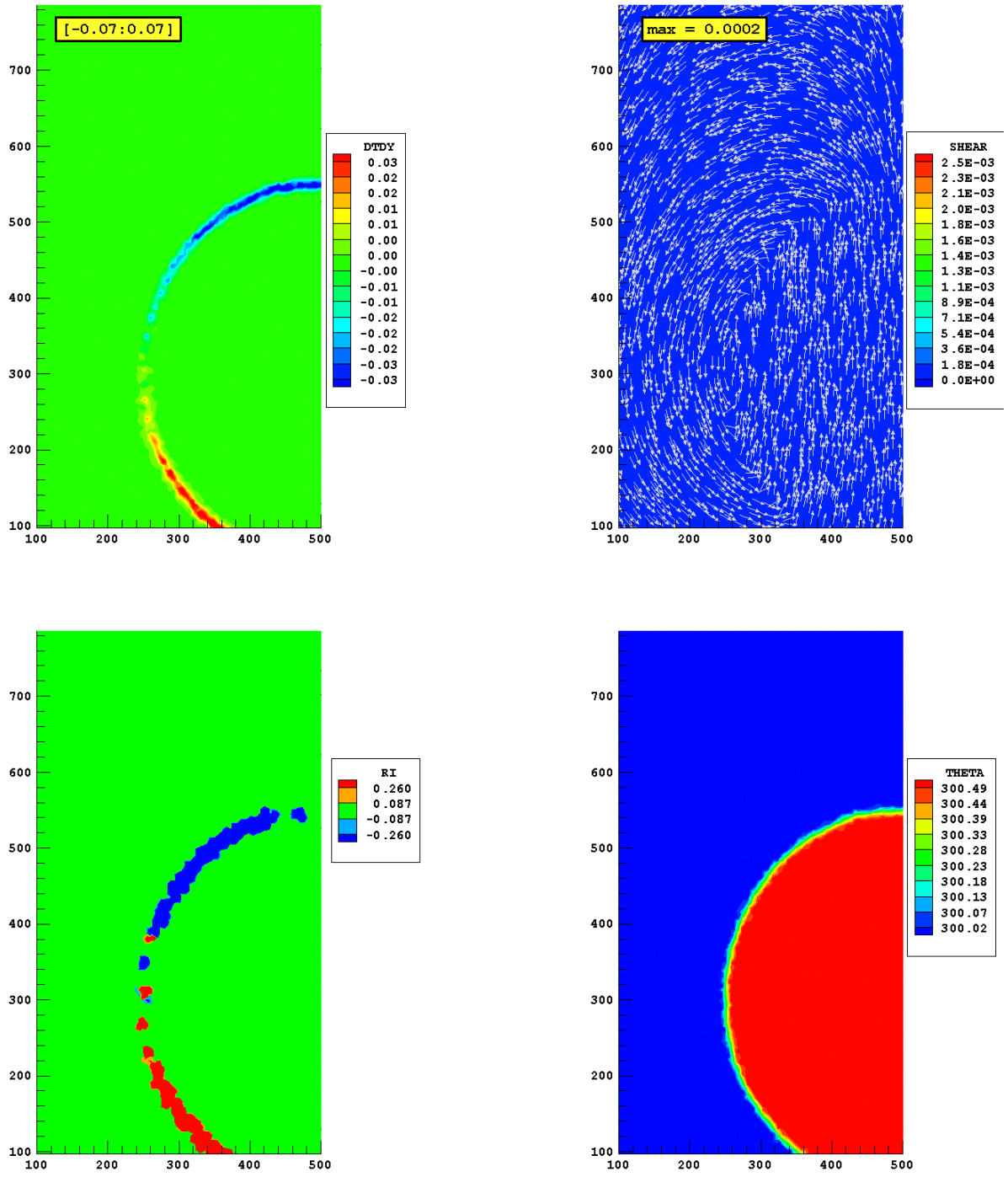

Figure 9. Potential temperature gradient (top left), shear (top right), Richardson number (bottom left) and potential temperature (bottom right). Time = 14 s.

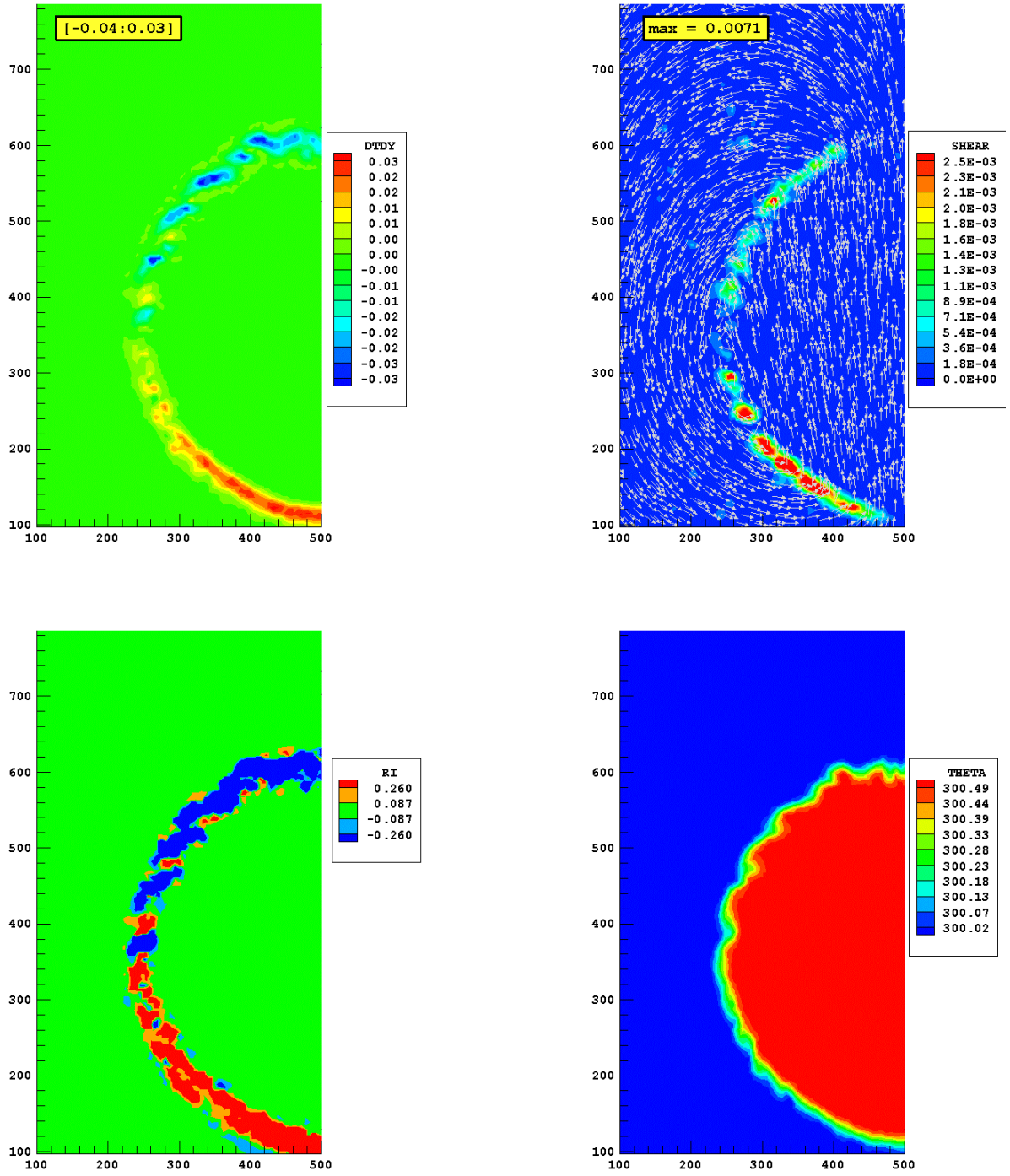

Figure 10. Potential temperature gradient (top left), shear (top right), Richardson number (bottom left) and potential temperature (bottom right). Time = 145 s.

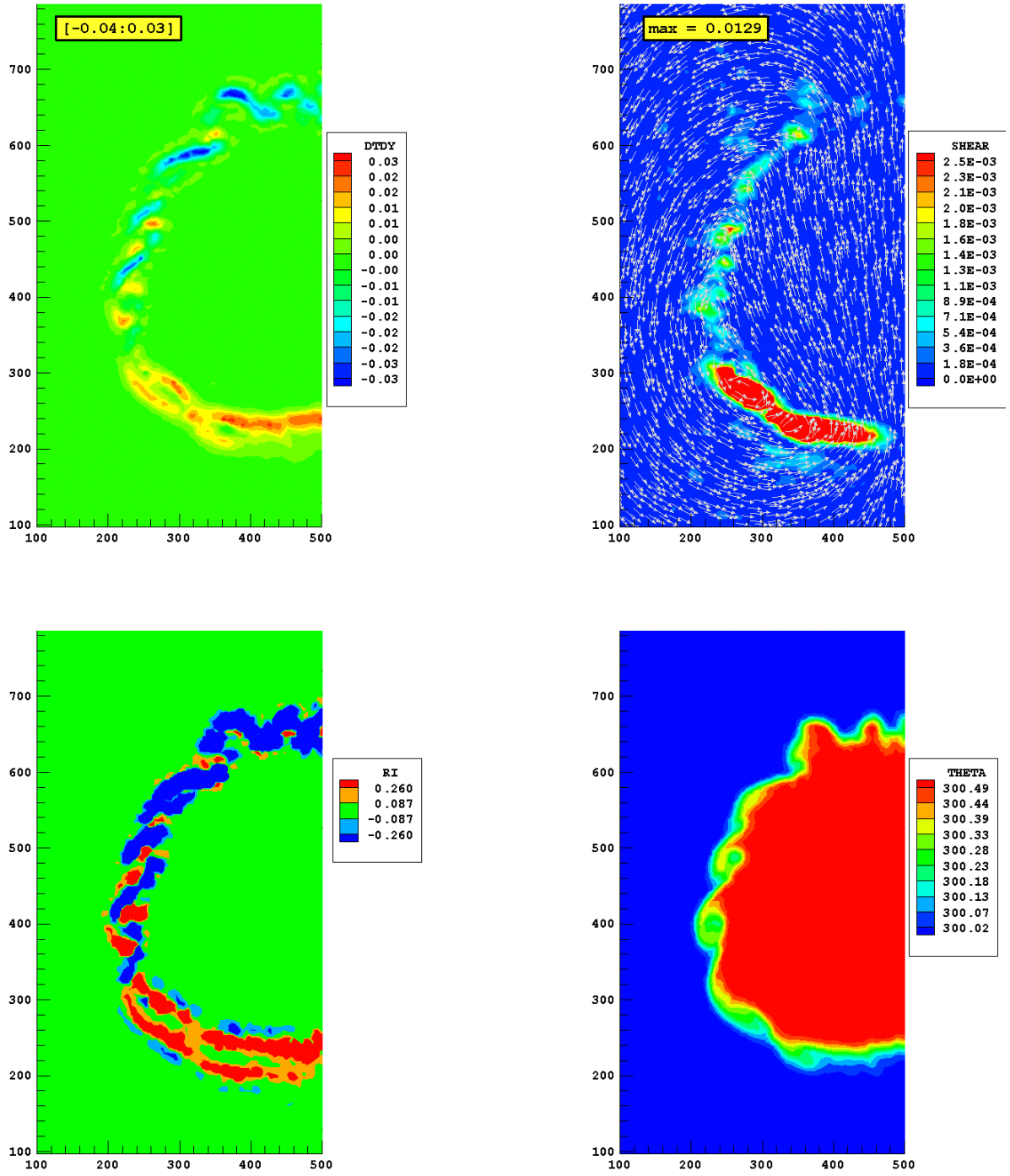

Figure 11. Potential temperature gradient (top left), shear (top right), Richardson number (bottom left) and potential temperature (bottom right). Time = 217 s.

Appendix

Godunov's method and its higher-order extensions have been designed for hyperbolic conservation laws. It is shown that the set of one-dimensional Euler equations governing the atmospheric flow are hyperbolic and thus an attempt can be made to apply the family of high-resolution numerical methods, which have been developed specifically for solving hyperbolic conservation laws. The Euler equations are written in a quasi-linear form,

$$U_t + A(U)U_x = 0 \tag{A.1}$$

The subscripts *t* and *x* denote derivatives in time and space respectively, and **A(U)** is the Jacobian matrix defined as,

$$A(U) = \begin{bmatrix} \frac{\partial f_1}{\partial u_1} & \frac{\partial f_1}{\partial u_2} & \frac{\partial f_1}{\partial u_3} \\ \frac{\partial f_2}{\partial u_1} & \frac{\partial f_2}{\partial u_2} & \frac{\partial f_2}{\partial u_3} \\ \frac{\partial f_3}{\partial u_1} & \frac{\partial f_3}{\partial u_2} & \frac{\partial f_3}{\partial u_3} \end{bmatrix} \tag{A.2}$$

The Jacobian matrix can be found by expressing the components of the flux vector **F** in terms of the components of the **U** vector of conserved variables:

$$F(U) = \begin{bmatrix} u_2 \\ \frac{u_2^2}{u_1} + C_o u_3^{\gamma} \\ \frac{u_2 u_3}{u_1} \end{bmatrix} \tag{A.3}$$

After some algebraic manipulations, the matrix in Eq. (A.2) simplifies to:

$$A(U) = \begin{bmatrix} 0 & 1 & 0 \\ -u^2 & 2u & a^2/\theta \\ -u\theta & \theta & u \end{bmatrix} \tag{A.4}$$

where, *a* is the speed of sound.

Proposition 1: The one-dimensional Euler equations governing the atmospheric flows are hyperbolic.
Proof. The eigenvalues of the Jacobian matrix **A(U)** are found by setting,

$$\left| A(U) - \lambda I \right| = 0 \tag{A.5}$$

Where, λ_i are the eigenvalues and **I** is the identity matrix. The solution of the resulting polynomial gives the following eigenvalues:

$$\lambda = \begin{bmatrix} u - a \\ u \\ u + a \end{bmatrix} \tag{A.6}$$

Since all eigenvalues are real, the system is hyperbolic.

Proposition 2: The K^2 characteristic field is linearly degenerate and the K^1 and K^3 characteristic fields are genuinely non-linear.

The right eigenvectors of the system can be derived by solving for:

$$K = \begin{bmatrix} k_1 & k_2 & k_3 \end{bmatrix}^T \tag{A.7}$$

such that,

$$AK = \lambda K \tag{A.8}$$

The right eigenvectors of the system are:

$$K^1 = \begin{bmatrix} 1 \\ u-a \\ \theta \end{bmatrix}; \qquad K^2 = \begin{bmatrix} 1 \\ u \\ 0 \end{bmatrix}; \qquad K^3 = \begin{bmatrix} 1 \\ u+a \\ \theta \end{bmatrix}. \tag{A.9}$$

Proof. Since,

$$\nabla\lambda_1(U)\cdot K^1 \neq 0; \qquad \nabla\lambda_2(U)\cdot K^2 = 0; \qquad \nabla\lambda_3(U)\cdot K^3 \neq 0 \tag{A.10}$$

It follows that the K^2 characteristic field is *linearly degenerate* which implies that the wave associated with it is a *contact discontinuity*. Whereas, the *genuinely non-linear* K^1 and K^3 fields will have waves, which can either be *rarefactions* (smooth waves) or *shocks* (discontinuities).

References

[1]Bacon, D. P., et al, "A Dynamically Adapting Weather and Dispersion Model: The Operational Multiscale Environment Model with Grid Adaptivity (OMEGA)", *Monthly Weather Review*, Vol. 128, 2000, pp. 2044-2076.

[2]Barth, T. J., and D. C. Jesperson, "The Design and Application of Upwind Schemes on Unstructured Meshes", AIAA Paper 1989-0366.

[3]Batten, P., M. A. Leschziner and U. C. Goldberg, "Average-State Jacobians and Implicit Methods for Compressible Viscous and Turbulent Flows", *Journal of Computational Physics*, Vol. 137, 1997, pp 38-78.

[4]Baum, J. D., H. Luo, and R. Löhner, "Numerical simulation of a blast inside a Boeing 747", AIAA Paper 1993-3091.

[5]Behrens, J., K. Dethloff, W. Hiller, and A. Rinke, "Evolution of Small-Scale Filaments in an Adaptive Advection Model for Idealized Tracer Transport", *Monthly Weather Review*, Vol. 128, 2000, pp. 2976-2982.

[6]Boris, J. and D. L. Book, "Flux-Corrected Transport. I. SHASTA, A Fluid Transport Algorithm that Works", *Journal of Computational Physics*, Vol. 11, 1973, pp. 38-69.

[7]Boybeyi, Z. N. Ahmad, D. Bacon, T. Dunn, M. Hall, P. Lee, A. Sarma and T. Wait, "Evaluation of the Operational Multiscale Environment Model with Grid Adaptivity against the European Tracer Experiment", *Journal of Applied Meteorology*, Vol. 40, 2001, pp. 1541-1558.

[8]Boybeyi, Z., S. Raman, and P. Zanetti, "Numerical investigation of possible role of local meteorology in Bhopal gas incident", *Atmospheric. Environment*, Vol. 29, 1995, pp. 479-496.

[9]Brooks, H. E. and C. A. Doswell III, "Extreme winds in high-precipitation supercells", Preprints of the *17th Conf. On Severe Local Storms*, Saint Louis, Missouri, 1993, pp. 173-177.

[10]Carpenter, R. L., K. K. Droegemeier, P. R. Woodward and C. E. Hane, **"**Application of the Piecewise Parabolic Method (PPM) to Meteorological Modeling", *Monthly Weather Review*, Vol. 118, 1990, pp. 586-612.

[11]Collela, P., and P. R. Woodward, "The Piecewise Parabolic Method (PPM) for Gas-Dynamical Simulations", *Journal of Computational Physics*, Vol. 54, 1984, pp. 174-201.

[12]Doswell, C., "Kinematic Analysis of Frontogenesis Associated with a Nondivergent Vortex", *Journal of Atmospheric Science*, 41, 1984, pp. 1242-1248.

[13]Durran, D. R., "The third-order Adams-Bashforth method: An attractive alternative to leapfrog time differencing", *Monthly Weather Review*, Vol. 119, 1991, pp. 702-720.

[14]Ghorai, S., A. S. Tomlin, and M. Berzins, "Resolution of pollutant concentrations in the boundary layer using a fully 3D adaptive gridding technique", *Atmospheric Environment,* Vol. 34, 2000, pp. 2851-2863.

[15]Godunov, S. K., "A Finite Difference Method for the Computation of Discontinous Solutions of the Equations of Fluid Dynamics", *Mat. Sb.*, Vol. 47, 1959, pp. 357-393.

[16]Gopalakrishnan, S. G., et al, "An Operational Multiscale Hurricane Forecasting System", *Monthly Weather Review*, Vol. 130, 2002, pp. 1830-1847.

[17]Harten, A., "High resolution schemes for hyperbolic conservation laws", *Journal of Computational Physics*, Vol. 49, 1983, pp. 357-393.

[18]Holmes, D. G., and S. D. Connell, "Solution of the 2D Navier-Stokes Equations on Unstructured Adaptive Grids", AIAA Paper 89-1932.

[19]Hourdin, F., and A. Armengaud, "The Use of Finite-Volume Methods for Atmospheric Advection of Trace Species. Part I: Test of Various Formulations in a General Circulation Model", *Monthly Weather Review*, Vol. 127, 1999, pp. 822-837.

[20]Hubbard, M. E., "Multidimensional slope limiters for MUSCL-type finite volume schemes on unstructured grids", *Journal of Computational Physics*, Vol. 155, 1999, pp. 54-74.

[21]Hubbard, M. E. and N. Nikiforakis, "A three-dimensional, adaptive, Godunov-type model for global atmospheric flows", *Monthly Weather Review*, Vol. 131, 2003, pp. 1848-1864.

[22]Ibáñez, J. M., and J. M. Martí, "Riemann solvers in relativistic astrophysics", *J. Comp. Appl. Math.*, Vol. 109, 1999, pp. 173-211.

[23]Jameson, A., W. Schmidt, and E. Turkel, "Numerical Solution of the Euler Equations by Finite Volume Method using Runge-Kutta Time Stepping Schemes", AIAA Paper 1981-1259.

[24]Koračin, D., V. Isakov and L. Mendez-Nuñez, "A cloud-resolving model with the radiation scheme based on the Monte Carlo method", *Atmospheric Research*, Vol. 47, 1998, pp. 437-459.

[25]Lilly, D. K., "On the Numerical Simulation of Buoyant Convection", *Tellus*. Vol. 14, 1962, pp. 148-172.

[26]Lin, S. J., W. C. Chao, Y. C. Sud, and G. K. Walker, "A class of van Leer-type transport schemes and its application to the moisture transport in a general circulation model", *Monthly Weather Review*, Vol. 122, 1994, pp. 1575-1593.

[27]Löhner, R., "Applied CFD Techniques: An Introduction based on Finite Element Methods", John Wiley and Sons Ltd., 2001.

[28]Löhner, R., "An Adaptive Finite Element Scheme for Transient Problems in CFD", *Computer Methods in Applied Mechanics and Engineering*. Vol. 61, 1987, pp. 323-338.

[29]Luo, H., J. D. Baum, and R. Löhner, "Extension of HLLC Scheme for Flows at all Speeds", AIAA Paper 2003-3840.

[30]Luo, H., J. D. Baum and R. Löhner, "A Fast, Matrix-free Implicit Method for Compressible Flows on Unstructured Grids", *Journal of Computational Physics*, Vol. 146, 1998, pp. 664-690.

[31]Ooyama, K. V., "A thermodynamic foundation for modeling the moist atmosphere", *Journal of Atmospheric Science*, Vol. 47, 1990, pp. 2580-2593.

[32]Pielke, R., et al, "A Comprehensive Meteorological Modeling System-RAMS", *Meteorol. Atmos. Phys.,* Vol. 49, 1992, pp. 69-91.

[33]Pietrzak, J., "The Use of TVD Limiters for Forward-in-Time Upstream-Biased Advection Schemes in Ocean Modeling", *Monthly Weather Review*, Vol. 126, 1998, pp. 812-830.

[34]Sharov, D. and K. Nakahashi, **"**Reordering of 3-D Hybrid Unstructured Grids for Vectorized LU-SGS Navier-Stokes Computations", AIAA Paper 1997-2102.

[35]Shaw, B. L., R. A. Pielke and C. L. Ziegler, "A Three-Dimensional Numerical Simulation of a Great Plains Dryline", *Monthly Weather Review*, Vol. 125, 1997, pp. 1489-1506.

[36]Skamarock, W. C., J. B. Klemp and J. Dudhia, "Prototypes for the WRF (Weather Research and Forecasting) Model", *2001 AMS Mesoscale Processes Conference*.

[37]Smagorinsky, J., **"**General Circulation Experiments With the Primitive Equations", *Monthly Weather Review,* Vol. 91, 1963, pp. 99-164.

[38]Smolarkiewicz, P. K., "A fully multidimensional positive definite advection transport algorithm with small implicit diffusion", *Journal of Computational Physics*, Vol. 54, 1984, pp. 325-362.

[39]Suratanakavikul, V. and A. J. Marquis, **"**A Comparative Study of Flux-Limiters in Unsteady and Steady Flows", *Proceedings of the 13th National Mech. Engr. Conf*, 1999.

[40]Toro, E. F., M. Spruce, and W. Speares, **"**Restoration of the Contact Surface in the HLL Riemann Solver", *Shock Waves*, Vol. 4, 1994, pp. 25-34.

[41]Toro, E. F., **"**Riemann Solvers and Numerical Methods for Fluid Dynamics", Springer-Verlag, 1999.

[42]Tremback, C. J., J. Powell, W. R. Cotton and R. Pielke, "The Forward-in-Time Upstream Advection Scheme: Extension to Higher Orders", *Monthly Weather Review*, Vol. 115, 1987, pp. 540-555.

[43]Van Leer, B., **"**Towards the Ultimate Conservative Difference Scheme. V. A Second-Order Sequel to Godunov's Method", *Journal of Computational Physics*, Vol. 32, 1979, pp. 101-136.

[44]Van Leer, B., **"**An Introduction to the Article "Reminiscences about Difference Schemes" by S. K. Godunov", *Journal of Computational Physics*, Vol. 153, 1999, pp. 1-5.

[45]Vásquez-Cendón, M. E., "Improved Treatment of Source Terms in Upwind Schemes for the Shallow Water Equations in Channels with Irregular Geometry", *Journal of Computational Physics*, Vol. 148, 1999, pp. 497-526.

[46]Venkatakrishnan, V., **"**On the Accuracy of Limiters and Convergence to Steady State Solutions", AIAA Paper 1993-0880.

[47]Xia, J., W. S. Lewellen and D. C. Lewellen, **"**Influence of Mach Number on Tornado Corner Flow Dynamics", Submitted to *Journal of Atmospheric Science,* 2003.